7. D. Bhattacharya and E. P. van den Heuvel [*Phys. Rep.* **203**, 1 (1991)] provide a comprehensive review of LMXB and MSP evolution. The AIC model for production of MSPs directly from collapse of WDs was proposed to solve the possible LMXB versus MSP birthrate problem in globulars by J. Grindlay and C. Bailyn [*Nature* **336**, 48 (1988)].
8. F. Camilo, D. R. Lorimer, P. Freire, A. G. Lyne, R. N. Manchester, *Astrophys. J.* **535**, 975 (2000).
9. The Chandra X-ray Observatory is described by M. Weisskopf, S. O'Dell, and L. van Speybroeck [*Proc. SPIE* **2805**, 142 (1996)]; the ACIS detector system is described by G. Garmire, J. Nousek, and M. Bautz (in preparation).
10. P. Hertz, J. Grindlay, *Astrophys. J.* **275**, 105 (1983).
11. F. Verbunt, R. Elson, J. van Paradijs, *Mon. Not. R. Astron. Soc.* **210**, 899 (1984).
12. P. C. Freire *et al.*, *Mon. Not. R. Astron. Soc.*, in press (e-Print available at http://xxx.lanl.gov/abs/astro-ph/0103372).
13. The core radius, r_c, is defined as the radius at which the projected surface brightness has decreased by a factor of two from its peak central value. It is a measure of central stellar density and can be related to cluster dynamical parameters [see (*1*)]. The most reliable determination of $r_c = 23''$ for 47Tuc is given by J. H. Howell, P. Guhathakurta, and R. L. Gilliland [*Publ. Astron. Soc. Pac.* **112**, 1200 (2000)].
14. F. Verbunt and G. Hasinger [*Astron. Astrophys.* **336**, 895 (1998)] report the results of the x-ray survey of 47Tuc carried out with the German-U.S. x-ray telescope ROSAT and its HRI detector.
15. Wavdetect is a source detection tool employing wavelet smoothing to match the expected point spread function. Along with the spectral analysis package, Sherpa, used for spectral fits to the brighter (≳300 ct) sources, it is part of the Chandra Interactive Analysis Operation (CIAO) developed by the Chandra X-ray Center (CXC) for analysis of Chandra data and available at http://asc.harvard.edu/ciao/.
16. M. Zoccali *et al.*, *Astrophys. J.* **553**, 733 (2001); e-Print available at http://xxx.lanl.gov/abs/astro-ph/0101485.
17. A two-dimensional K-S test method to detect overlapping but statistics-limited sources has been developed by S. Metchev and J. Grindlay [*Astrophys. J.*, in preparation]; maximum likelihood methods are used in (*14*).
18. W. Becker, J. Trumper, *Astron. Astrophys.* **341**, 803 (1999).
19. J. Grindlay, P. Edmonds. C. Heinke, F. Camilo, P. Freire, in preparation.
20. R. E. Rutledge, L. Bildsten, E. F. Brown, G. G. Pavlov, V. E. Zavlin, *Astrophys. J.*, **551**, 921 (2001); e-Print available at http://xxx.lanl.gov/abs/astro-ph/0012400.
21. C. Heinke, J. Grindlay, P. Edmonds, in preparation. Spectral models fit to the cluster sources included both continuum (black body, bremsstrahlung, and power law) and emission line (Raymond-Smith collisional excitation) models, as provided in the CIAO analysis package [see (*15*)].
22. P. Edmonds, R. Gilliland, J. Grindlay, C. Heinke *et al.*, in preparation.
23. M. Garcia *et al.*, *Astrophys. J.*, **553**, L47 (2001); e-Print available at http://xxx.lanl.gov/abs/astro-ph/0012452.
24. B. Warner, *Cataclysmic Variables*, (Cambridge Univ. Press, Cambridge, 1995).
25. A. Zdjiarski [*ASP Conf. Series* **161**, 16 (1999)] provides a recent review.
26. R. Giacconni *et al.*, *Astrophys. J.* **551**, 624 (2001); e-Print available at http://xxx.lanl.gov/abs/astro-ph/0007240.
27. A. van Teesling, K. Beurmann, and F. Verbunt [*Astron. Astrophys.* **315**, 467 (1996)] suggest absorption by the disk in high inclination nonmagnetic CVs, whereas accretion curtain absorption in magnetic systems is proposed by C. Hellier [*ASP Conf. Ser.* **157**, 1 (1999)].
28. F. Paresce, G. de Marchi, F. Ferraro, *Nature* **360**, 46 (1992).
29. P. Edmonds *et al.*, *Astrophys. J.* **468**, 241 (1996).
30. M. Auriere, L. Koch, S. Ortolani, *Astron. Astrophys.* **214**, 113 (1989).
31. C. Knigge, M. Shara, D. Zurek, K. Long, R. Gilliland, e-Print available at http://xxx.lanl.gov/abs/astro-ph/0012187.
32. D. Minniti *et al.*, *Astrophys. J.* **474**, L27 (1997).
33. M. Shara, L. Bergeron, R. Gilliland, A. Saha, R. Petro, *Astrophys. J.*, **471**, 804 (1996).
34. P. Edmonds *et al.*, in preparation.
35. K. Horne, *ASP Conf. Ser.* **157**, 349 (1999).
36. R. Dempsey, J. Linsky, T. Fleming, J. Schmitt, *Astrophys. J.* **478**, 358 (1997).
37. R. Di Stefano, S. Rappaport, *Astrophys. J.* **423**, 274 (1994).
38. J. Grindlay, *ASP Conf. Ser.* **157**, 377 (1999); P. Edmonds *et al.*, *Astrophys. J.* **516**, 250 (1999).
39. F. A. Rasio, E. D. Phahl, S. Rappaport, *Astrophys. J.* **532**, L47 (2000).
40. E. Pfahl, S. Rappaport, *Astrophys. J.*, **550**, 172 (2001); e-Print available at http://xxx.lanl.gov/abs/astro-ph/0009212.
41. E. Quataert, R. Narayan, *Astrophys. J.* **520**, 298 (1999).
42. D. Calzetti, G. DeMarchi, F. Paresce, M. Shara, *Astrophys. J.* **402**, L1 (1993); G. De Marchi, F. Paresce, M. Stratta, R. Gilliland, R. Bohlin, *Astrophys. J.*, **468**, L51 (1996).
43. S. F. Portegies Zwart, S. McMillan, *Astrophys. J.* **528**, L17 (2000).

44. P. Guhathakurta, B. Yanny, D. Schneider, J. Bahcall, *ASP Conf. Series* **50**, 303 (1993).
45. We thank F. Camilo, H. Cohn, and R. Gilliland for helpful comments. This observation was conducted as part of the GTO program on the Chandra X-ray Observatory with support from NASA (HRC contract NAS8-38248).

28 March 2001; accepted 9 May 2001
Published online 17 May 2001;
10.1126/science.1061135
Include this information when citing this paper.

Spike Transmission and Synchrony Detection in Networks of GABAergic Interneurons

Mario Galarreta[1]* and Shaul Hestrin[1,2]

The temporal pattern and relative timing of action potentials among neocortical neurons may carry important information. However, how cortical circuits detect or generate coherent activity remains unclear. Using paired recordings in rat neocortical slices, we found that the firing of fast-spiking cells can reflect the spiking pattern of single-axon pyramidal inputs. Moreover, this property allowed groups of fast-spiking cells interconnected by electrical and γ-aminobutyric acid (GABA)–releasing (GABAergic) synapses to detect the relative timing of their excitatory inputs. These results indicate that networks of fast-spiking cells may play a role in the detection and promotion of synchronous activity within the neocortex.

In vivo studies indicate that coherent firing among cortical neurons may be related to sensory stimulation and behavioral states (*1–4*). However, how postsynaptic cells read out the pattern of activity of their presynaptic axons and how spike synchrony among input axons may be detected by the cortical network remain poorly understood (*3*, *5*).

Studies in intact animals as well as theoretical work suggest that inhibitory interneurons may coordinate neuronal activity in cortical networks (*6–11*). Fast-spiking (FS) cells are a prominent subtype of GABA-releasing (GABAergic) interneurons (*12*), exerting powerful inhibitory control of both excitatory and inhibitory cortical cells (*13–17*). The properties of excitatory synapses at FS cells (*13*, *18*), as well as their voltage-dependent conductances (*19–21*), suggest that these cells may be particularly sensitive to the timing of their inputs, as has been shown for hippocampal interneurons (*22*, *23*). Moreover, cortical networks of FS cells are interconnected by electrical synapses (*14*, *15*, *17*, *24*), and these electrical connections can promote synchronous spiking (*14*, *15*). We investigated how the presynaptic pattern of firing can be transmitted through single-axon pyramidal-to-FS connections and how the degree of synchrony among excitatory inputs may be detected by groups of FS cells.

Precise timing of spike transmission. Pairs of pyramidal and FS cells were recorded in rat neocortical slices (*25*). Monosynaptic pyramidal–FS cell connections were detected by the generation of short-latency unitary excitatory postsynaptic potentials (EPSPs) in response to individual pyramidal spikes (mean latency, 0.63 ± 0.05 ms; range, 0.4 to 1.0 ms; $n = 12$ pairs) (*26*). To reproduce the ongoing synaptic activity that occurs in vivo (*27*), we injected into the postsynaptic FS cells fluctuating current waveforms that changed from trial to trial, resulting in an irregular firing of ~5 to 50 Hz (Fig. 1A,

[1]Department of Comparative Medicine, [2]Department of Neurology and Neurological Sciences, Stanford University School of Medicine, Stanford, CA 94305, USA.

*To whom correspondence should be addressed. E-mail: galarreta@stanford.edu

middle panels) (*28*). The impact of a presynaptic spike on the postsynaptic firing (that is, spike transmission) was studied by producing a timed action potential in the pyramidal cell with every trial (Fig. 1A, upper panel). Spike transmission was examined by constructing a peristimulus time histogram (PSTH) of the postsynaptic cell. This revealed a sharp increase in the firing frequency of the FS cell after the presynaptic spike (Fig. 1A, lower panel, and Fig. 1B). We defined the temporal precision of spike transmission as the width (10 to 90 %) of the PSTH peak (*29*). The average temporal precision in seven pairs was 1.5 ± 0.3 ms (Fig. 1D), and the latency between the peaks of the presynaptic spike and of the PSTH was 1.7 ± 0.1 ms (n = 7 pairs). We also defined the spike transmission gain (STG) as the area of the PSTH peak. STG represents the average number of spikes added in the postsynaptic cell by a single presynaptic action potential. In seven pairs, the STG ranged from 0.046 to 0.711 (Fig. 1C). We found an approximately linear relationship between the STG and the amplitude of the unitary EPSP [r = 0.98 (Fig. 1C)]. Thus, under our experimental conditions, the STG per 1-mV EPSP was ~0.04. High temporal precision was not limited to large synaptic inputs. Small inputs were unreliable, but the postsynaptic spikes they produced were precisely timed (Fig. 1D).

We next examined the temporal relationship between the PSTH peak and the waveforms of the corresponding single-axon excitatory postsynaptic current (EPSC) and EPSP (Fig. 2, A and B) (*30*). The duration of the PSTH peak was much shorter than that of the unitary EPSP (Fig. 2B), as previously shown in spinal motoneurons (*31*). The PSTH peak occurred during the rise time or peak of the EPSP and, on average, preceded the peak of the EPSP by 0.37 ± 0.2 ms (n = 7 pairs). The

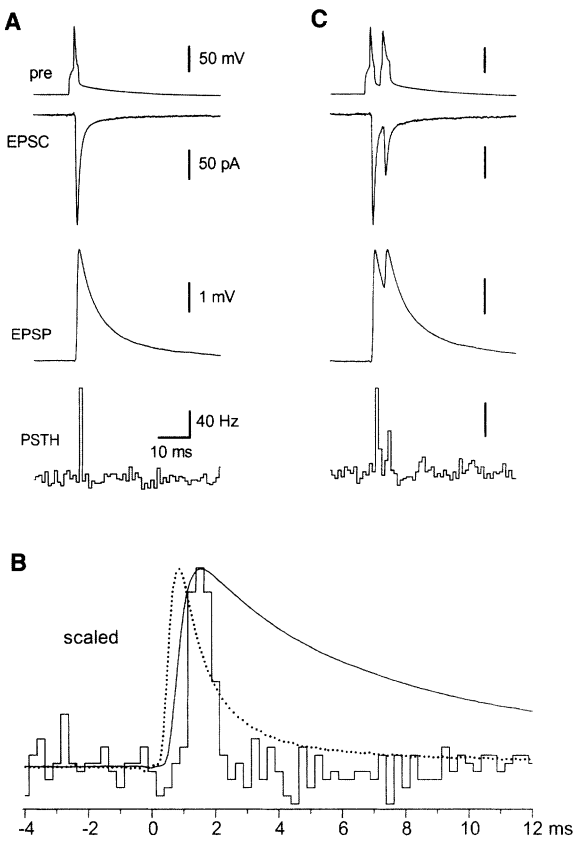

Fig. 2. Pyramidal-to-FS cell connections can preserve the pattern of presynaptic inputs with millisecond precision. (**A**) Comparison of the time course of a single-axon EPSC (top) (holding potential = −70 mV, average of 50 traces), the corresponding single-axon EPSP recorded near resting conditions (middle) (V_m = −79 mV, average of 100 traces), and the resulting PSTH (bottom) (n = 560 trials, bin width = 1 ms). These three traces have been scaled, superimposed, and expanded in (**B**), where the value of 0 on the time scale corresponds to the presynaptic spike peak. The polarity of the unitary EPSC (dotted line) has been reversed (binning of the PSTH is 250 μs). (**C**) Two presynaptic action potentials separated by an interval of 4 ms (top) produced two independent peaks in the postsynaptic PSTH (bottom) (n = 685 trials, bin width = 1 ms). Middle traces show corresponding single-axon EPSCs (holding potential = −70 mV, average of 50 traces) and EPSPs. Data were obtained from the same connection shown in (A).

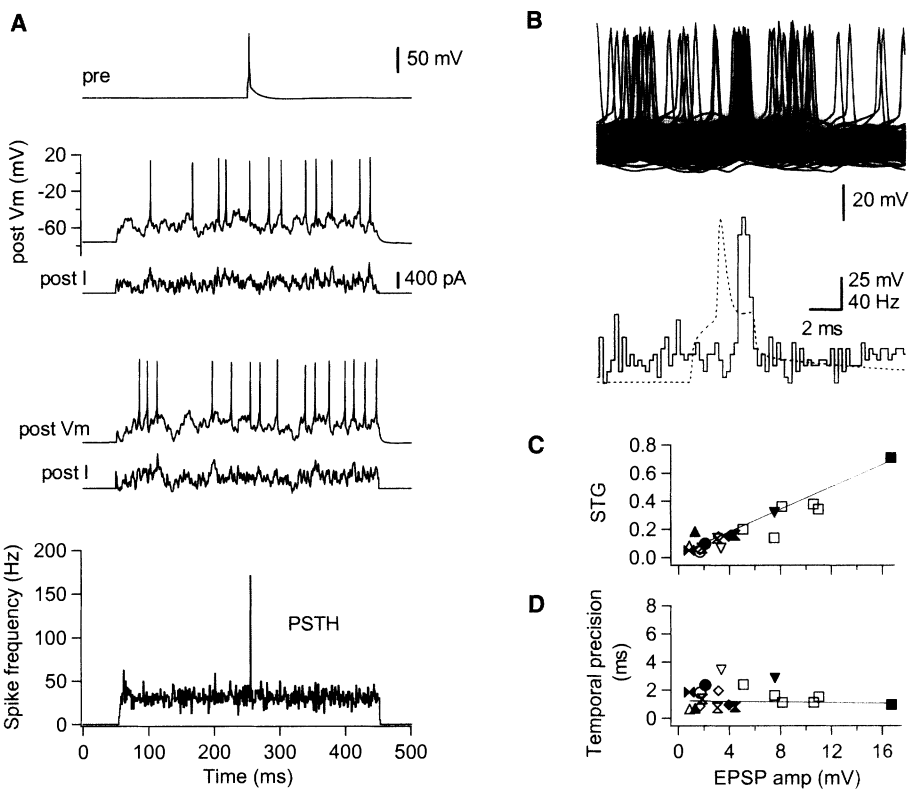

Fig. 1. Properties of spike transmission at pyramidal-to-FS cell connections. (**A**) Irregular spike activity [postsynaptic membrane potential (V_m)] was generated in a postsynaptic FS cell by injecting pulses of random signals (post I) (*28*). Two examples of these injections are shown in the middle panels. A single spike in the presynaptic pyramidal cell (top) produced a sharp peak in the FS cell PSTH (bottom) (n = 560 trials, bin width = 1 ms). (**B**) (Top) Superposition of 75 consecutive postsynaptic recordings at an expanded time scale. (Bottom) Temporal relationship between the peak of the PSTH and the presynaptic spike (superimposed dashed line, bin width = 250 μs). The width of the PSTH was 0.9 ms (10 to 90 %), and the latency between both peaks was 1.4 ms. Data are from the same pair shown in (A). (**C**) Linear relationship between the amplitude of the single-axon EPSP and the STG (r = 0.98). (**D**) Lack of correlation (r = −0.09) between the EPSP amplitude (amp) and the temporal precision of spike transmission. Solid symbols in (C) and (D) represent data obtained from seven different pairs at basal presynaptic stimulation frequencies (0.33 to 1 Hz). Open symbols illustrate additional data obtained from the same pairs by means of paired-pulse protocols. Data from a given pair are plotted with symbols of the same shape.

high temporal precision of spike transmission in these connections could allow the firing of postsynaptic cells to reflect the temporal pattern of presynaptic spikes. We thus generated in the presynaptic cell two action potentials separated by a brief interval, and found that the postsynaptic PSTH showed two independent peaks [n = 3 pairs; interval, 4 to 7 ms (Fig. 2C)]. The second PSTH peak was smaller in amplitude, reflecting paired-pulse depression, and was in agreement with a linear relationship between EPSP amplitude and STG (Fig. 1C). Thus, spike transmission at pyramidal-to-FS cell connections can transfer high-frequency signals and preserve the pattern of the presynaptic inputs.

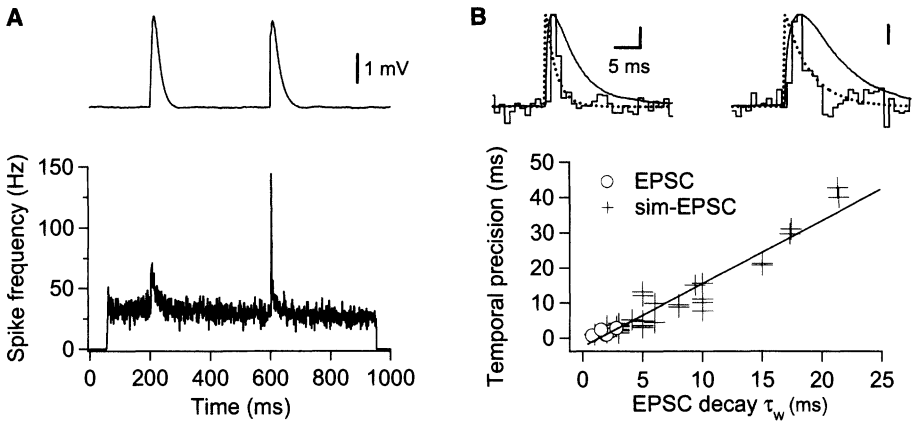

Fig. 3. The kinetics of the synaptic currents are important for synaptic integration of spike transmission. (**A**) PSTH (n = 1800 trials, bin width = 1 ms) obtained from an FS cell in response to the coinjection of synthetic current waveforms and two simulated EPSPs of different rise times (8 ms versus 1 ms) but similar decay time courses (upper trace). (**B**) Relationship between the decay time constant of single-axon EPSCs or sim-EPSCs and the width of the PSTH peak (10 to 90%, r = 0.96). The upper traces illustrate the different PSTH peaks obtained by two sim-EPSCs (dashed lines) with similar rise times but different decay time constants of 2 ms (left) and 5 ms (right). The corresponding sim-EPSPs are shown superimposed (continuous lines). Left vertical calibration bar: 13 pA, 0.35 mV, and 8.5 Hz. Right vertical calibration bar: 9 pA, 0.35 mV, and 6 Hz.

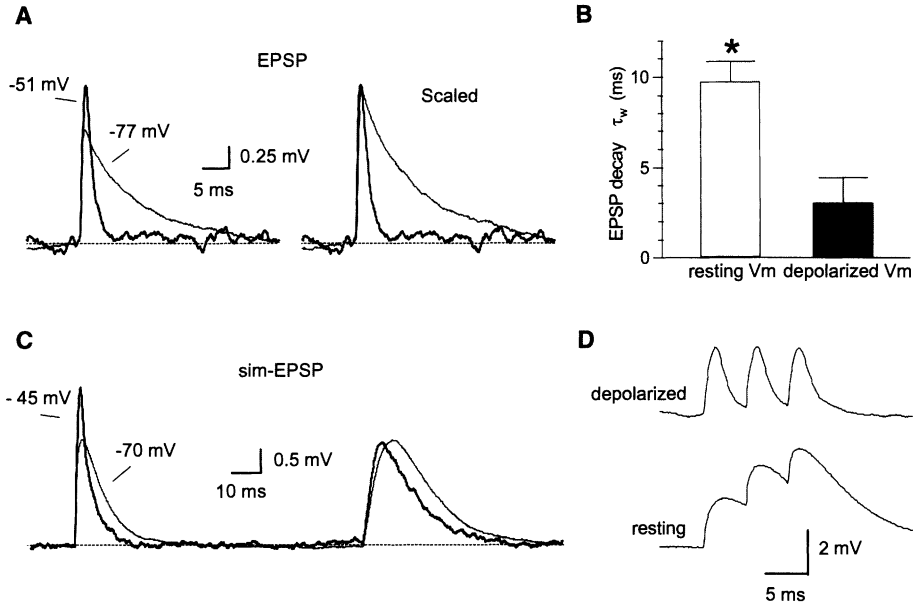

Fig. 4. Pyramidal-to-FS cell EPSPs decay faster near threshold potentials. (**A**) Superimposition of the time course of a pyramidal-to-FS cell unitary EPSP recorded at resting V_m (thin trace, –77 mV) and a depolarized V_m (thick trace, –51 mV). The traces (average of 150 trials) are shown scaled in the right panel. (**B**) Faster decay time course of unitary EPSP at depolarized versus resting V_m (n = 5 pairs, $P < 0.02$). (**C**) Superimposition of sim-EPSPs with fast (1.1 ms, left) and slow (6.4 ms, right) rise times recorded at resting (thin trace) and near-threshold potentials (thick trace) in a FS cell. Each trace is the average of 60 traces. (**D**) Three sim-EPSPs (10 to 90%, rise time = 1.1 ms, decay τ = 6.3 ms, 200 Hz) recorded from a FS cell at resting (V_m = –70 mV) and depolarized (V_m = –33 mV) potentials. Each trace is the average of 40 trials.

EPSC kinetics and temporal precision. The rate of membrane depolarization may affect the efficacy of spike-generating mechanisms (*32*, *33*), and this could contribute to the discrepancy between the shape of the EPSP and the PSTH peak. We thus simulated synaptic potentials (sim-EPSPs) of variable kinetics by injecting depolarizing current waveforms into the FS cell (*34*). Two sim-EPSPs of similar amplitudes and decay time courses but different rise times (10 to 90% = 1 ms versus 8 ms) produced different effects on the cell spiking activity [n = 4 cells (Fig. 3A)]. Because fast-decaying single-axon EPSCs are correlated with fast-rising EPSPs (*35*) (n = 6 pairs; r = 0.88), we next examined the relationship between the EPSC decay time constant and the temporal precision of spike transmission (Fig. 3B). The temporal precision was correlated with the decay time constants of both synaptic EPSCs and sim-EPSCs [r = 0.96 (Fig. 3B)] (*36*). These results indicate that the kinetics of the postsynaptic currents can affect the temporal precision of spike transmission.

Depolarization induces EPSP acceleration and boosting. At excitatory synapses among pyramidal neurons, depolarization of the postsynaptic cell slows down the EPSP time course (*23*, *37*–*39*). FS cells, however, express voltage-dependent conductances distinct from those of principal neurons (*19*–*21*). Moreover, at hippocampal interneurons, the EPSPs time course is relatively insensitive to membrane depolarization (*23*). Thus, we compared the time course of pyramidal-to-FS–cell unitary EPSPs recorded at resting and near-threshold potentials (Fig. 4A) (*40*). The decay time course of FS single-axon EPSPs at depolarized potentials (–48 ± 1 mV) was faster than that of the synaptic inputs recorded at resting potentials [–73 ± 2 mV, n = 5 pairs (Fig. 4A)]. The weighted decay time constant of EPSPs at the resting potential was 9.7 ± 1.1 ms as compared to 3.0 ± 1.4 ms at depolarized membrane potential [n = 5 pairs, paired t test, $P < 0.02$ (Fig. 4B)] (*41*). Using sim-EPSPs, we also examined whether the shape of the events could affect their voltage-dependent modification. We compared fast- (~1 ms) and slow-rising (~5 to 10 ms) sim-EPSPs and found that fast-rising events, similar to single-axon EPSPs, were selectively modified at near-threshold potentials. Their amplitude was boosted by 54% ($P < 0.001$, n = 6 experiments) and their decay accelerated by 37% ($P < 0.05$, n = 6 experiments). Slow-rising events did not show significant changes [$P >$ 0.05 (Fig. 4C)]. Tetrodotoxin (0.5 μM) prevented the boosting and reduced the acceleration of fast-rising events, indicating the involvement of voltage-dependent Na^+ channels in these modifications [$P < 0.01$, n = 5 (*42*)]. The depolarization-induced accelera-

tion of the EPSP time course may have a profound effect on temporal summation (Fig. 4D). At resting potential, a 200-Hz train of three sim-EPSPs exhibited summation, whereas at depolarized potential, the acceleration prevented the summation. These findings suggest that the temporal properties of spike transmission at pyramidal-to-FS cell connections reflect the fast kinetics of their postsynaptic receptors (*43*, *44*) as well as voltage-dependent conductances (*19–21*, *23*, *45*).

Synchrony detection in interneuron networks. The temporal precision of spike transmission that we describe here may allow groups of FS cells interconnected by electrical and GABAergic synapses (*14*, *15*, *17*) to be sensitive to synchronous excitatory inputs. When a pair of FS cells is coupled only electrically (Fig. 5A, bottom), a presynaptic spike generated a biphasic response consisting of a brief depolarization [reflecting the spike itself (open arrow)] and a slower hyperpolarizing component [reflecting the presynaptic AHP (solid arrow)] in the postsynaptic cell. If the cells are connected by GABAergic synapses, a hyperpolarizing inhibitory postsynaptic potential (IPSP) is produced (Fig. 5A, top) (*46*). When both types of connections coexist, nearly synchronous inputs into different FS cells will be aided by the mutual depolarizing phase of the electrical response, and synchronous spiking will be promoted (*14*, *15*). On the other hand, nonsynchronous inputs will be relatively inefficient, because FS cells receiving late inputs would be influenced by the hyperpolarizing response, mediated by both GABAergic and electrical connections, from neurons receiving early inputs. We recorded from pairs of FS cells connected by both electrical and GABAergic synapses (Fig. 5B). We created sim-EPSPs by injecting EPSC-like waveforms in both cells, and depolarized the cells so that individual sim-EPSPs would generate a spike in 50 to 70 % of the trials. Next, we tested whether the relative timing of two independent inputs could affect the spiking of the FS cells. When the time interval between the sim-EPSPs at each cell was 0 to 1 ms, both FS cells fired with higher probability within a narrow time window (Fig. 5C). Under these conditions, the probability of firing increased by 33 ± 10% (n = 3 pairs, $P <$ 0.05). In contrast, when the two inputs were separated by an interval of 5 ms, the firing of the cell receiving the delayed input was reduced by 59 ± 20% [$P < 0.05$ (Fig. 5D)].

FS cells receive strong thalamocortical inputs (*15*) as well as corticocortical and local excitatory inputs (*13*, *18*, *47–49*) and form networks with other FS cells interconnected by both GABAergic and electrical synapses (*14*, *15*, *17*, *24*). Here we provide evidence that the temporal characteristics of spike transmission and the properties of electrical and GABAergic synapses could endow networks of FS cells with sensitivity to the synchrony of their excitatory inputs. These properties would allow a group of FS cells to fire in synchrony when receiving coincident excitatory inputs. Given that FS cells make inhibitory contacts with both pyramidal and nonpyramidal neurons (*13–17*, *48*, *50–52*), the simultaneous firing of several FS cells could then coordinate the activity of their postsynaptic cells (*7*). Thus, we propose that local networks of FS cells could play a role in the readout and transmission of information that may be encoded by the synchronous activity of excitatory neurons.

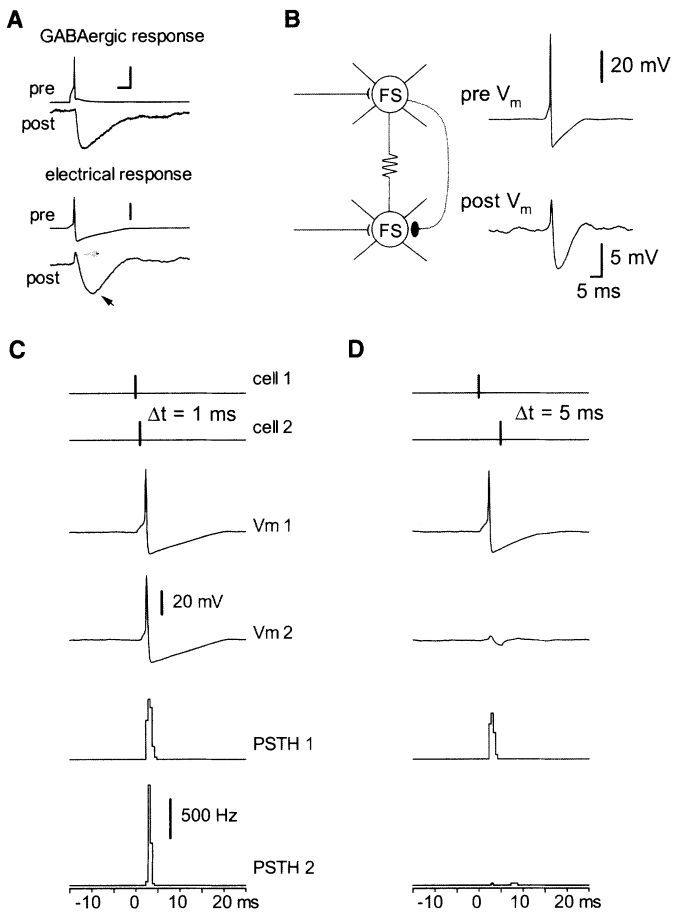

Fig. 5. Precise spike transmission of excitatory inputs allows pairs of FS cells connected by both GABAergic and electrical synapses to detect synchronous activity. (**A**) (Upper traces) Example of an isolated single-axon GABAergic IPSP (calibration bars: vertical, 50 mV and 1 mV; horizontal, 5 ms). (Lower traces) Postsynaptic response (post-V_m = –37 mV) produced by a spike in the presynaptic neuron (pre-V_m = –40 mV) in a pair of FS cells connected exclusively by electrical synapses (DC coupling coefficient, 10.1 %; calibration bar, 30 and 0.5 mV). (**B**) Recordings from a pair of FS cells connected by both electrical and GABAergic synapses (left, schematic drawing). A presynaptic spike produces a biphasic response in the postsynaptic cell (pre-V_m = −38 mV, post-V_m = −35 mV). (**C**) Two sim-EPSPs separated by 1 ms (schematically represented in the top traces) produced the synchronous firing of both FS cells (PSTH bin = 0.5 ms). (**D**) If two sim-EPSPs are separated by 5 ms, the firing of the postsynaptic cell is dramatically reduced. Δt represents the interval between sim-EPSPs.

References and Notes

1. C. M. Gray, W. Singer, *Proc. Natl. Acad. Sci. U.S.A.* **86**, 1698 (1989).
2. E. Vaadia *et al.*, *Nature* **373**, 515 (1995).
3. W. Singer, *Neuron* **24**, 49 (1999).
4. P. N. Steinmetz *et al.*, *Nature* **404**, 187 (2000).
5. M. N. Shadlen, W. T. Newsome, *J. Neurosci.* **18**, 3870 (1998).
6. G. Buzsaki, J. J. Chrobak, *Curr. Opin. Neurobiol.* **5**, 504 (1995).
7. J. G. Jefferys, R. D. Traub, M. A. Whittington, *Trends Neurosci.* **19**, 202 (1996).
8. J. Csicsvari, H. Hirase, A. Czurko, G. Buzsaki, *Neuron* **21**, 179 (1998).
9. H. A. Swadlow, I. N. Beloozerova, M. G. Sirota, *J. Neurophysiol.* **79**, 567 (1998).
10. M. S. Jones, K. D. MacDonald, B. Choi, F. E. Dudek, D. S. Barth, *J. Neurophysiol.* **84**, 1505 (2000).
11. I. Timofeev, F. Grenier, M. Steriade, *Proc. Natl. Acad. Sci. U.S.A.* **98**, 1924 (2001).
12. Y. Kawaguchi, Y. Kubota, *Cereb. Cortex* **7**, 476 (1997).
13. M. Galarreta, S. Hestrin, *Nature Neurosci.* **1**, 587 (1998).
14. M. Galarreta, S. Hestrin, *Nature* **402**, 72 (1999).
15. J. R. Gibson, M. Beierlein, B. W. Connors, *Nature* **402**, 75 (1999).
16. A. M. Thomson, D. C. West, J. Hahn, J. Deuchars, *J. Physiol.* **496**, 81 (1996).
17. G. Tamas, E. H. Buhl, A. Lorincz, P. Somogyi, *Nature Neurosci.* **3**, 366 (2000).
18. J. R. Geiger, J. Lubke, A. Roth, M. Frotscher, P. Jonas, *Neuron* **18**, 1009 (1997).
19. M. Martina, P. Jonas, *J. Physiol.* **505**, 593 (1997).
20. M. Martina, J. H. Schultz, H. Ehmke, H. Monyer, P. Jonas, *J. Neurosci.* **18**, 8111 (1998).
21. A. Chow *et al.*, *J. Neurosci.* **19**, 9332 (1999).
22. R. Miles, *J. Physiol.* **428**, 61 (1990).
23. D. Fricker, R. Miles, *Neuron* **28**, 559 (2000).
24. L. Venance *et al.*, *Proc. Natl. Acad. Sci. U.S.A.* **97**, 10260 (2000).
25. Sprague-Dawley rats of both sexes (15 to 19 days old) were anesthetized by an intraperitoneal injection of ketamine [87 mg per kilogram of body weight (mg/kg)] and xylazin (13 mg/kg) and decapitated. The dissection and maintenance of neocortical slices was

as described in (*14*), except that 4 mM lactic acid, 2 mM pyruvic acid, and 0.4 mM ascorbic acid were added to the extracellular solution, and 1 mM kynurenic acid was added during the dissection. Pairs of pyramidal neurons and FS cells were recorded in layer V of the visual and somatosensory cortices. Somatic whole-cell recordings were made as previously described in (*14*), except that the intracellular solution contained 0.2 mM EGTA. Data are given as mean ± SEM. Differences were considered statistically significant (Student's t test) if $P < 0.05$. Peaks in the cross-correlogram were considered significant if individual bins exceeded expected values by 2.5 SDs.

26. The latency of the single-axon EPSPs was measured between the peak of the presynaptic action potential and the beginning of the synaptic potential. Average synaptic responses were obtained after aligning the traces by the peak of the presynaptic action potential. Spikes were generated in the pyramidal cells by injecting a brief pulse (3 to 5 ms, 1 nA) of current.
27. Z. F. Mainen, T. J. Sejnowski, *Science* **268**, 1503 (1995).
28. To generate the uncorrelated random currents, a Poisson train (2000 Hz) was convolved with the waveform of a single-axon EPSC, and the result was combined with the convolution of a Poisson train (1000 Hz) and a single-axon IPSC waveform. The waveforms of the synaptic currents were previously recorded (*13*). Trials were separated by 1 to 3 s.
29. PSTHs were built from 200 to 1300 trials. Data were aligned to the peak of the presynaptic spike before constructing the PSTH. To determine the beginning and the end of the PSTH peak, a cumulative sum of the histogram was built after subtracting the baseline spike frequency (*31*). The baseline was defined as a 50-ms period preceding the presynaptic spike.
30. At a holding potential of −70 mV, presynaptic spikes produced unitary EPSCs with an average rise time (10 to 90 %) of 0.43 ± 0.06 ms and a weighted decay time constant of 1.9 ± 0.3 ms [n = 6 pairs (Fig. 2A)]. The mean peak amplitude was 185 ± pA (range, 28 to 488 pA; n = 6 pairs). The corresponding unitary EPSPs recorded at resting conditions (~ −73 mV) had a rise time of 0.77 ± 0.12 ms and a weighted decay time constant of 9.4 ± 0.9 ms [n = 7 pairs (Fig. 2A)]. The mean peak amplitude was 5.3 mV (range, 0.9 to 16.7 mV). The decay time course of unitary EPSCs and EPSPs was fitted with a biexponential function. The weighted decay time constant was calculated as $\tau_w = \tau_1 \times A_1 + \tau_2 \times A_2$, where τ_1 and τ_2, and A_1 and A_2 represent, respectively, the time constant and relative amplitude of each exponential component.
31. T. C. Cope, E. E. Fetz, M. Matsumura, *J. Physiol.* **390**, 161 (1987).
32. C. E. Stafstrom, P. C. Schwindt, J. A. Flatman, W. E. Crill, *J. Neurophysiol.* **52**, 244 (1984).
33. R. Azouz, C. M. Gray, *Proc. Natl. Acad. Sci. U.S.A.* **97**, 8110 (2000).
34. The sim-EPSP with a fast-rising phase was produced by injecting current according to the following equation: $y = A_1[1 - \exp(-t/\tau_{rise1})][\exp(-t/\tau_{decay1})] + A_2[1 - \exp(-t/\tau_{rise2}][\exp(-t/\tau_{decay2}]$, in which y is the amplitude of the injected current, t is time, A_1 = 150 pA, τ_{rise1} = 0.01 ms, τ_{decay1} = 1 ms, A_2 = 70 pA, τ_{rise2} = 3 ms, and τ_{decay2} = 20 ms. To generate the slow-rising sim-EPSP, current was injected according to the following equation: $y = A[1 - \exp(-t/\tau_{rise})] \times [\exp(-t/\tau_{decay})]$, in which A = 150 pA, τ_{rise} = 10 ms, and τ_{decay} = 15 ms.
35. In six pyramidal-to-FS cell connections, both the EPSP and its corresponding EPSC were recorded. A significant correlation between the EPSC decay time constant and the EPSP rise time was observed.
36. Simulated EPSPs with a fast rise time (~0.1 to 0.2 ms, 10 to 90%) and variable decay time courses were generated by injecting current according to the equation $y = A[1 - \exp(-t/\tau_{rise})] \times [\exp(-t/\tau_{decay})]$.
37. C. E. Stafstrom, P. C. Schwindt, M. C. Chubb, W. E. Crill, *J. Neurophysiol.* **53**, 153 (1985).
38. A. M. Thomson, D. Girdlestone, D. C. West, *J. Neurophysiol.* **60**, 1896 (1988).
39. G. Stuart, B. Sakmann, *Neuron* **15**, 1065 (1995).
40. Near-threshold unitary EPSPs were obtained by depolarizing the membrane of the postsynaptic FS cell with square current pulses of 400 ms.
41. The average amplitude of the unitary EPSPs at resting conditions was 0.9 ± 0.1 mV, and at depolarized potentials, it was 1.1 ± 0.2 mV (n = 5 pairs, P = 0.07).
42. M. Galarreta, S. Hestrin, data not shown.
43. J. R. Geiger *et al.*, *Neuron* **15**, 193 (1995).
44. B. Lambolez, N. Ropert, D. Perrais, J. Rossier, S. Hestrin, *Proc. Natl. Acad. Sci. U.S.A.* **93**, 1797 (1996).
45. M. Martina, I. Vida, P. Jonas, *Science* **287**, 295 (2000).
46. GABA-mediated IPSPs were isolated from the signal mediated via electrical synapses by subtracting the responses obtained at depolarized potentials with those obtained near Cl^- reversal potential.
47. E. H. Buhl *et al.*, *J. Physiol.* **500**, 689 (1997).
48. A. Reyes *et al.*, *Nature Neurosci.* **1**, 279 (1998).
49. M. C. Angulo, J. Rossier, E. Audinat, *J. Neurophysiol.* **82**, 1295 (1999).
50. G. Tamás, E. H. Buhl, P. Somogyi, *J. Physiol.* **500**, 715 (1997).
51. G. Tamás, P. Somogyi, E. H. Buhl, *J. Neurosci.* **18**, 4255 (1998).
52. A. Gupta, Y. Wang, H. Markram, *Science* **287**, 273 (2000).
53. We thank W. T. Newsome for useful comments on the manuscript. Supported by NIH grants EY09120 and EY12114.

6 April 2001; accepted 10 May 2001

Liquid Crystal Alignment on Carbonaceous Surfaces with Orientational Order

J. Stöhr,[1]* M. G. Samant,[1] J. Lüning,[1]* A. C. Callegari,[2] P. Chaudhari,[2] J. P. Doyle,[2] J. A. Lacey,[2] S. A. Lien,[2] S. Purushothaman,[2] J. L. Speidell[2]

We used near-edge x-ray absorption fine structure (NEXAFS) spectroscopy to link the orientational bond order at three carbonaceous surfaces—rubbed polyimide, ion beam–irradiated polyimide, and ion beam–irradiated diamond-like carbon films—with the direction of liquid crystal (LC) alignment on these surfaces. We show that, in general, LC alignment can be created on any carbonaceous substrate by inducing orientational order at its surface. Our results form the scientific basis for LC alignment layers consisting of amorphous carbon films in which orientational order near the surface is induced by a directional low-energy ion beam.

The alignment of a nematic LC, consisting of an assembly of rodlike molecules, on rubbed polymer surfaces underlies the manufacture of today's flat panel displays (*1*). Because of various problems associated with the wet polymer deposition and the mechanical rubbing processes, much research has been devoted to the development of improved methods and materials. So far, this effort has been largely unsuccessful. Although noncontact methods such as ultraviolet (*2*–*4*) or ion beam (IB) (*5*) irradiation have been suggested, their reliance on polymer substrates has impeded their technological use. A replacement process should be based on an inexpensive substrate material that can be deposited in a dry deposition process on large area panels, required for future applications in desk-top displays. Also, present displays suffer from limited viewing angles, and an improved process should allow the fabrication of microscopic multidomain alignment regions that enable larger viewing angles (*4*). The lack of scientific understanding of the alignment process is another critical factor that has been missing for a device enabling advance.

Early LC alignment models were based on the existence of microgroves at the surface of the alignment film (*6*). Later models invoked epitaxylike effects at the polymer surface where the LC is oriented by a preferred crystalline structure (*7*), microcrystalline nucleation sites (*8*), or crystalline regions with a preferred chain orientation (*9*). The technologically important pretilt angle has been speculated to arise from tilted main or side chain segments at the rubbed polymer surface that "guide" the LC rods (*10*, *11*).

Theoretical advances have been impeded by the complexity of the LC-polymer system, and only specific aspects of the alignment phenomenon have been addressed. The preferred orientation of the LC rods parallel to the surface has been attributed to steric effects between the LC and a flat surface (*12*), and their preferred uni-

[1]IBM Research Division, Almaden Research Center, 650 Harry Road, San Jose, CA 95120, USA. [2]IBM Research Division, T. J. Watson Research Center, Post Office Box 218, Yorktown Heights, NY 10598, USA.

*Present address: Stanford Synchrotron Radiation Laboratory, Post Office Box 20450, Mail Stop 69, Stanford, CA 94309, USA.